CHAPTER - 4

Investigation of threshold anomaly in the near-barrier elastic scattering of ^{7}Li on ^{116}Sn

4.1 Introduction **86**

4.2 Experimental Description **88**

4.2.1 Energy Loss Calculations **89**

4.3 Experiment Details **89**

4.4 Electronics and Data acquisition **92**

4.5 Optical model analysis of the elastic scattering **93**

4.5.1 Analysis Using Phenomenological Woods-Saxon Potential **93**
4.5.2 Analysis Using the Double-Folding São Paulo Potential **101**

4.6 Total reaction cross sections **106**

4.7 Breakup threshold anomaly in ^{6,7}Li + ^{116}Sn system: A dispersion relation analysis **110**

4.8 Conclusions **113**

References **114**

Published in:

1. **N. N. Deshmukh** *et al., Investigation of the threshold anomaly in the near-barrier elastic scattering of ^{7}Li on ^{116}Sn*, Eur. Phys. J A **47**, 118 (2011).
2. **N. N. Deshmukh** *et al., Effect of breakup channels on the weakly bound, radioactive and halo nuclei using the reduction procedures*, Proceedings of National Conference on Emerging Interfaces of Physics and Technology – 2011 (EIPT – 2011), Excel India Publishers (ISBN: 978-93-81361-31-3), Page 108 – 111.
3. **N. N. Deshmukh** *et al., Threshold anomaly in the elastic scattering of weakly bound projectile ^{7}Li on the medium – mass target ^{116}Sn,* AIP Conference Proceedings, **1423**, 122 – 125 (2012) (IX – Latin America Symposium on Nuclear Physics and Applications, 2011).

4.1 Introduction

During the last few years, the scattering of weakly bound nuclei colliding at energies near and below the Coulomb barrier has been a subject of great interest. The energy dependence of the optical potential (OP) of the elastic scattering of tightly bound nuclei, at near barrier energies, show a rapid variation of both the real and imaginary parts of the potential. This energy dependence is produced by polarization potentials originated from the coupling between the elastic scattering and different reaction channels, such as inelastic excitations, transfer of nucleons, breakup etc. Dynamic polarization potential, or simply polarization potential, is such that when it is added to the bare energy independent potential, it produces the same elastic scattering cross section as the one obtained with coupled channel calculations. The net effect on the energy dependence of the optical potential depends on the importance and strength of the different specific polarization potentials. For systems containing only tightly bound nuclei, couplings to bound excited states or transfer channels produce an attractive polarization potential. This additional attraction of the real potential decreases the Coulomb barrier, consequently enhancing the fusion cross section, when compared with no-coupling calculations. This phenomenon has been named threshold anomaly (TA) [1–3]. The energy dependences of the real and imaginary potentials are related to each other and are consistent with a dispersion relation [1-3]. The basic characterization of the TA is the observation of a localized peak in the real part of the potential accompanying a sharp decrease of the imaginary part as the bombarding energy decreases towards the Coulomb barrier. The behaviour of the imaginary part of the potential is related with the closing of reaction channels when the energy approaches or is smaller than the Coulomb barrier.

When at least one of the colliding nuclei is weakly bound, the situation changes because the break-up channel may become important and this channel has excitation function that does not drop sharply at energies below the Coulomb barrier. Furthermore, the breakup channel feeds states in the continuum, that only under some spatial restrictions goes back to fusion. So, the net polarization potential in the scattering of weakly bound nuclei has two components: one attractive, due to the couplings of the elastic channel with inelastic excitations and other direct reactions and one repulsive, due to the breakup. If the attractive potential predominates, the behaviour of the net polarization potential is such that TA is still observed. However, if the

repulsive polarization potential predominates, one says that the system presents the Breakup Threshold Anomaly (BTA) [4,5]. In the original paper describing this phenomenon [5], it was mentioned that the BTA is characterized by the increase of the imaginary potential as the energy decreases towards the barrier. Nevertheless, BTA might also be interpreted as the absence of the TA due to the breakup channel [6], and consequently energy independent real and imaginary potentials.

The investigation of the presence of TA, BTA or energy independent optical potentials through the analysis of elastic scattering angular distributions is a very difficult task, since the desired manifestation of the optical potential behaviour can only be assessed at near and below barrier energies, where the elastic scattering is predominantly of the Rutherford type, and small deviations from it may only be obtained from very precise measurements. Even so, the low sensibility of the nuclear interacting potential at such low energies with the corresponding elastic scattering data leads to large error bars in the determination of such potentials. Satchler [2] has already addressed this difficulty and recently complementary measurements on that direction were adopted by Zerva et al. [7,8] by the backscattering technique.

In our previous work we have investigated the elastic scattering of the ^{6}Li + ^{116,112}Sn systems [9]. A clear BTA behaviour was observed, with the imaginary potential increasing when the bombarding energy decreases towards the barrier. This behaviour was found to be consistent with the systematic obtained from the elastic scattering of ^{6}Li on different targets, from ^{27}Al to ^{209}Bi (^{27}Al, ^{58}Ni, ^{64}Ni, ^{64}Zn, ^{90}Zr, ^{144}Sm, ^{208}Pb and ^{209}Bi) [4, 5, 10-17]. For the scattering of ^{7}Li the situation is not so clear. The ^{7}Li nucleus has breakup (α + t) threshold energy of 2.47 MeV and one bound excited state at 0.48 MeV. As pointed out by Lubian et al. [18], since ^{7}Li has one bound excited state and the stripping of one neutron may have large positive Q-values for several target nuclei, the attractive component of the dynamic polarization potential in the scattering of this projectile may be comparable or even predominates over the repulsive dynamic polarization potential due to the breakup. The net result may vary qualitatively for different targets, since the strengths and the interference between the different polarization potentials may be different. Actually, a systematic behaviour for the energy dependence of the optical potential in the scattering of ^{7}Li has not been reached so far, since the few systems investigated in the literature (^{27}Al, ^{28}Si, ^{59}Co, ^{138}Ba, ^{144}Sm, ^{208}Pb) [4, 15, 16, 19-24] show different behaviours. Particularly

for medium-heavy targets, there is only one work on the ^{144}Sm target [15], where nearly energy independent real and imaginary potentials were observed. For the ^{138}Ba target, different analyses lead to different conclusions [4, 23, 24].

In order to contribute to obtain a more clear picture of a possible systematic behaviour for the optical potential in the near barrier scattering of ^{7}Li [25], we performed measurements of elastic scattering for the ^{7}Li + ^{116}Sn system, also filling the gap between A = 59 and 144 for the target mass. The energy range of the measurements is from 20% below the Coulomb barrier to 70% above the barrier. The total reaction cross sections have also been extracted by the optical model fitting of the experimental data and they are compared with those from the ^{6}Li + ^{116}Sn system.

In this chapter we give experimental details of this work. Further, an optical model analysis of the measured elastic scattering angular distributions is presented in order to study the energy dependence of the interaction potential at near barrier energies. The derived reaction cross sections are compared with the ones for the ^{6}Li+ ^{116}Sn system and also with various weakly and tightly bound systems.

4.2 Experimental Description

The present thesis reports the experimental investigation on reaction mechanism carried out at the 14 UD Pelletron Accelerator set up as a collaborative project between the Bhabha Atomic Research Centre (BARC) and the Tata Institute of Fundamental Research (TIFR), has been serving as a major facility for heavy ion accelerator based research in India since its commissioning in December 1988. The precise description, except energy loss calculations, of accelerator facilities is described earlier in Chapter – 3, Section 3.2.

4.2.1. Energy Loss Calculations

When an energetic beam interacts with the target there is momentary electrostatic interaction between it and the atoms of the target by which it is passing. As a result of which it loses some energy in continuation with the elastic fragments, which loses partial or full energy in the ΔE detector. This energy loss is also of prime importance for the kinematical calculations and data analysis. The energy loss for the ^{7}Li in the targets and elastic fragments in the ΔE detector were calculated by using the program stopping power and range of ions in matter (SRIM) [26]. The amount of energy lost (ΔE) is inversely proportional to the beam energy and is given by the relation,

$$\frac{dE}{dx} \propto \frac{MZ^2}{E} \qquad (4.1)$$

The respective energy loss of the ^{7}Li beam in 430 μg/cm^2 ^{116}Sn target was 68 KeV.

4.3 Experiment Details

The experiment was performed at Bhabha Atomic Research Centre – Tata Institute of Fundamental Research (BARC–TIFR) pelletron facility, Mumbai, India. The beam of ^{7}Li was delivered by the 14UD Pelletron accelerator. The elastic scattering angular distributions were measured for ^{7}Li beam at ten different bombarding energies starting from below the Coulomb barrier, namely, 18, 19, 20, 21, 22, 23, 24, 26, 30 and 35 MeV. The nominal Coulomb barrier for this system is around 23 MeV in the laboratory frame. The beam was bombarded on a 430 μg/cm^2 self supported enriched ^{116}Sn (≥ 98%) target and the elastically scattered ^{7}Li ions were detected by a four solid state silicon surface barrier ΔE + E telescopic arrangement. The telescopes used were of different thicknesses (T_1 with ΔE = 40 μm and E = 1500 mm thick, T_2 with ΔE = 15 μm and E = 1500 mm thick, T_3 with ΔE = 25 μm and E = 1000 mm thick, and T_4 with ΔE = 25 μm and E = 1000 mm thick). One monitor of thickness 600 μm was used for the absolute normalization. The telescopes were placed on a rotating arm inside a 1 meter diameter scattering chamber at angular separation of 10° between consecutive telescopes. The monitor was fixed at the forward angle 30°. Beam currents were ranging between 7 and 40 nA. The angular distributions were measured in steps of 2.5° to 5° at angles from 20° to 173° at lower

energies and from 20° to 105° for higher energies. The uncertainty in the detector angular position is 0.1 degrees.

The statistical error in this system was found out to be less than 5% in the case of forward angles and a maximum of 30% in the case of backward angles. From the known abundances of the Sn target the contribution from the contaminants of the target was estimated to about 1%. The detectors solid angles uncertainty is 2%. When one adds the uncertainties in the angular position, in the beam angle and in the beam spot position one estimates the overall systematic uncertainty in the normalization as ± 6.0%. So, the overall errors in the cross sections are from 8.0% and 31%. A Photograph of the collaborators is posted below in Fig. 4.1 while setting up the experiment. Fig. 4.2 shows a typical bi-parametric E-ΔE spectrum for the $^{7}Li + ^{116}Sn$ system at E_{lab} = 35 MeV and $\theta = 40^{0}$. The inset of Fig.4.2 shows the corresponding projection for the Z = 3 events.

Figure 4.1 Collaborators along with the author doing experimental setup.

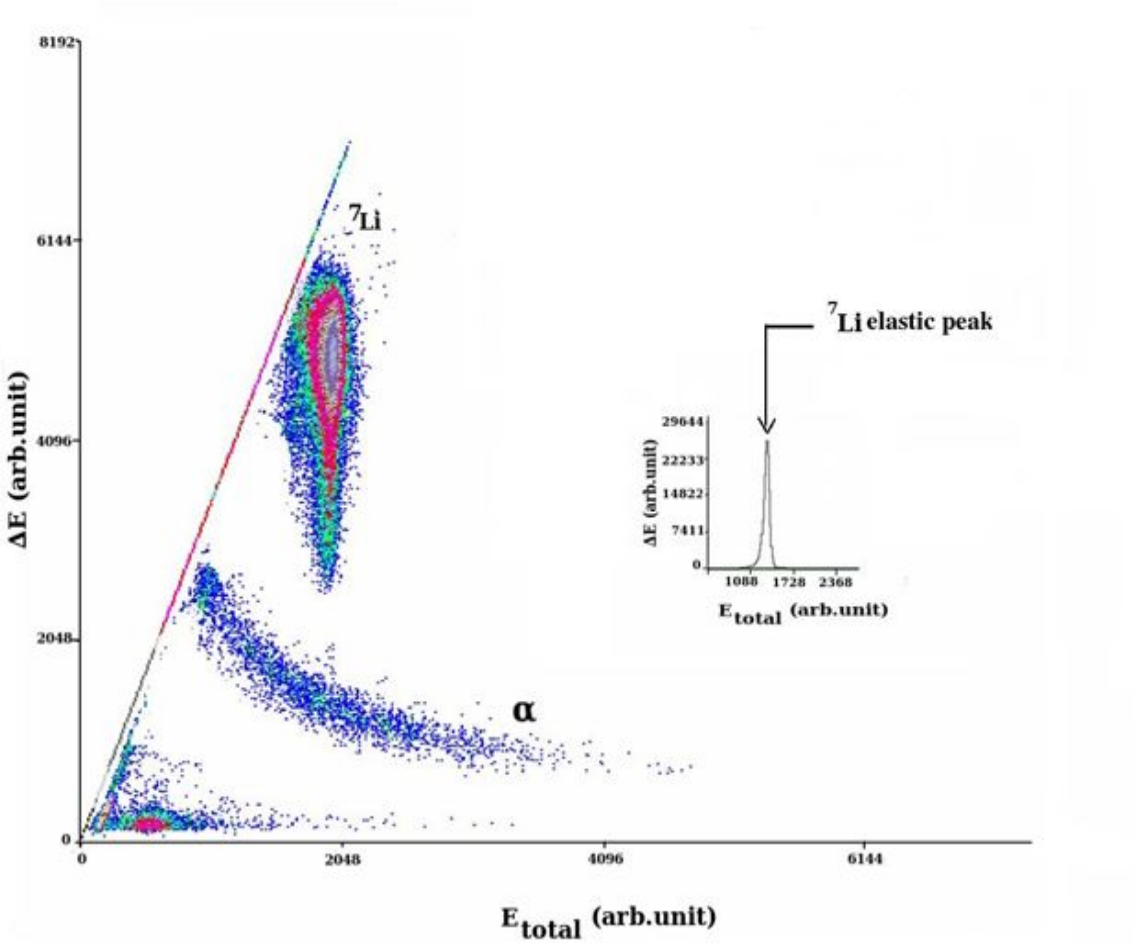

Figure 4.2 A typical bi-parametric E-ΔE spectrum for the ^{7}Li + ^{116}Sn system at E_{lab} = 35 MeV and θ = 40^{0}. The Projection of the ^{7}Li elastic peak of the bi-parametric E-ΔE spectrum is shown in the inset.

4.4 Electronics and data acquisition

The electronics setup is the same as we did it for ^{6}Li experiment with a difference of, an additional fourth detector, and the usage of only one monitor. The brief theoretical details and circuit diagram of it are given in the Chapter 3, section 3.4.

4.5 Optical model analysis of the elastic scattering

In this section we present the analysis of the elastic scattering angular distribution data. We use two different kinds of potential, in order to check the consistency of the results that should be model independent. In section 4.5.1 we describe the analysis with a phenomenological Woods-Saxon form interaction potential and in section 4.5.2 the analysis is performed by using the double-folding Sao Paulo potential (SPP) [27,28].

4.5.1. Analysis Using Phenomenological Woods-Saxon Potential

The phenomenological Woods – Saxon potential has been used to fit the elastic scattering angular distribution data by using the ECIS code [29]. The optical model potential used to extract the elastic scattering differential cross sections is given by the following equation.

$$U(r) = V_{coul}(r) - V_r f(r, R_r, a_r) - iW_i f(r, R_i, a_i) \qquad (4.2),$$

where V_{coul} is the Coulomb potential of a uniformly charged sphere of radius $R_c = 1.25 (A_p^{1/3} + A_t^{1/3})$ fm, A_p and A_t being the mass numbers of the projectile and target respectively; f represents the Woods-Saxon form function which is given by $f(r, R, a) = [1 + exp (r-R/a)]^{-1}$, where R is the radius and a is the diffuseness; r_i is the reduced radius, defined as $R_i = r_i (A_p^{1/3} + A_t^{1/3})$. Accordingly, the third term in equation (4.2) represents the volume imaginary potential of the optical potential U and W_i symbolizes its depth. The second term is the real part of the potential U, where V_r symbolizes its depth.

As we did not divide the imaginary part of the optical potential into two parts (volume + surface), the whole absorption due to the inelastic scattering, transfer channels, breakup and fusion processes is taken care by the volume imaginary potential of the optical potential U. This phenomenological framework contains six parameters i.e., V_r and W_i, namely, the two depths, R_r and R_i, namely, the two radii, a_r and a_i, namely, the two diffusenesses. These quantities may be free parameters to fit the experimental differential cross sections. However, by varying such a

large number of parameters one may obtain unrealistic physically values. Therefore, it is usual to keep some fixed parameters in the fit procedure.

The fitting procedure of the data was performed by changing only the real and imaginary depths of the potential and by keeping the real and imaginary reduced radii as 1.06 and 0.53 fm, respectively. After the first fit was obtained, we once again kept the radii fixed and varied the diffusivity of the potentials from 0.49 to 0.57 fm in steps of 0.02 fm and the depths of the real and imaginary potentials were fitted. For the lowest three energies, the diffuseness of the potentials was reduced to 0.45 fm in order to obtain attractive real nuclear potential and absorption of flux. As it usually happens in this kind of analysis, although very good fits were obtained, several families of optical potential parameters that describe the angular distributions fitted equally well the data. These ambiguities are removed by evaluating the potential at the sensitivity radii R_{Sr} and R_{Si} [2], corresponding to the real and imaginary potential, defined as the value of the radii for which different potentials with similar good fits have the same value. The derived mean sensitivity radii were 10.42 and 8.95 fm for real and imaginary potential, respectively. Fig. 4.3 (a) & (b) show, for the energy of 23 MeV, families of potentials that give similar fits, and the crossing points corresponding to the sensitivity radii for the real and imaginary parts, respectively. Finally the energy dependence of the interacting potentials were determined with an average sensitive radius R_S = 9.685 fm i.e., the average between R_{Sr} and R_{Si}, along with the mean diffuseness a = 0.53 fm for highest energies and a = 0.45 fm for lowest energies. Figs. 4.4 (a), (b) & (c), show the experimental elastic scattering angular distributions in the energy range E_{lab} = 18 – 35 MeV. The best fit obtained, with the parameters are shown in the Table 4.1. The corresponding values of the energy dependence of the interacting potentials are shown in Fig. 4.5. The error bars in Fig. 4.5 represent the range of deviation of the potential corresponding to a $\chi 2$ variation of one unit. For energies where $\chi 2$ is much larger than the unity (21 MeV, 24 MeV and 35 MeV), this criterion leads to unrealistic small error bars, as it can be observed in Fig. 4.5.

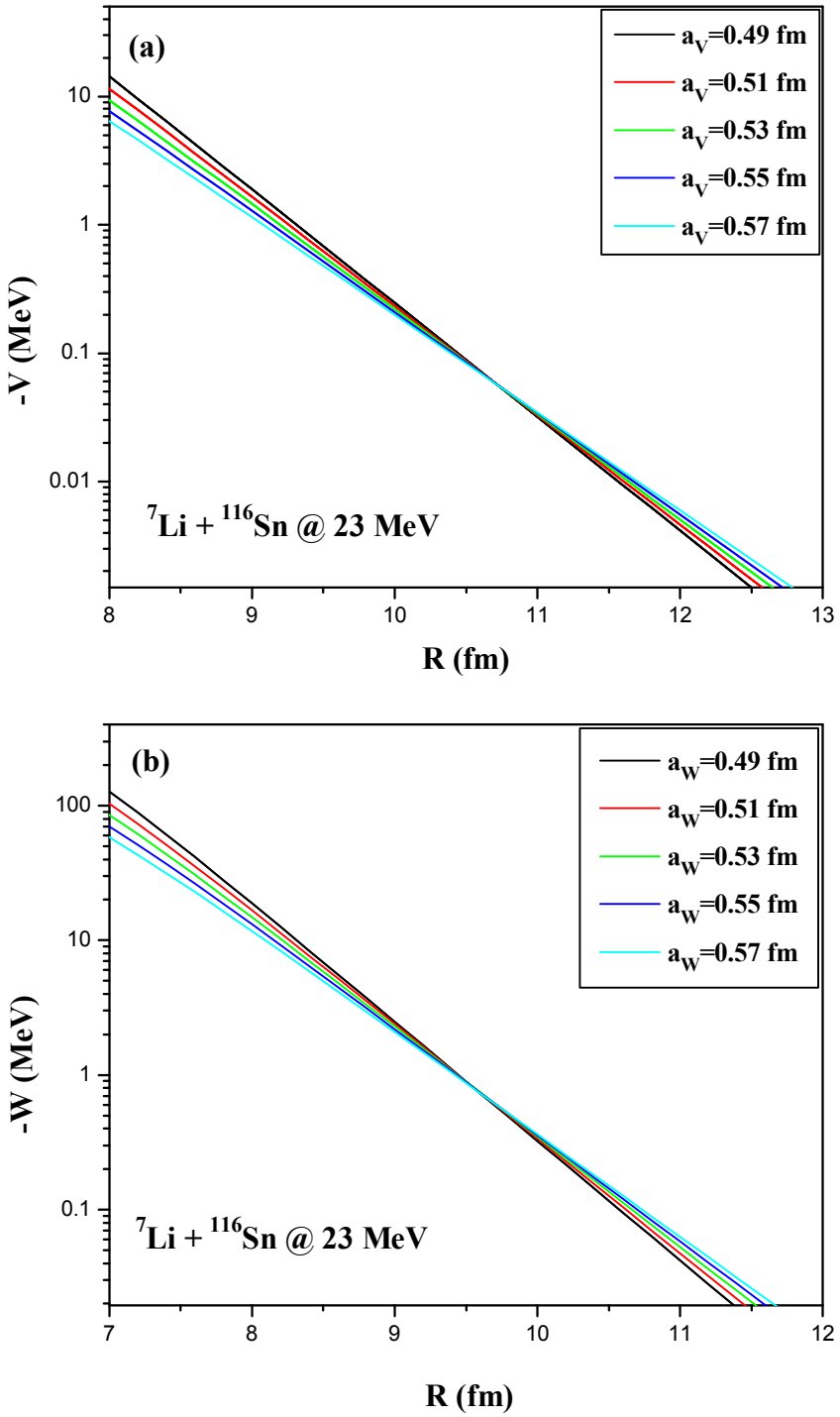

Figure 4.3 Different families of potential parameters that produce similar fits of the data, at 23 MeV. The real and imaginary sensitivity radii are the values where they intersect each other, respectively in Fig. (a) and (b).

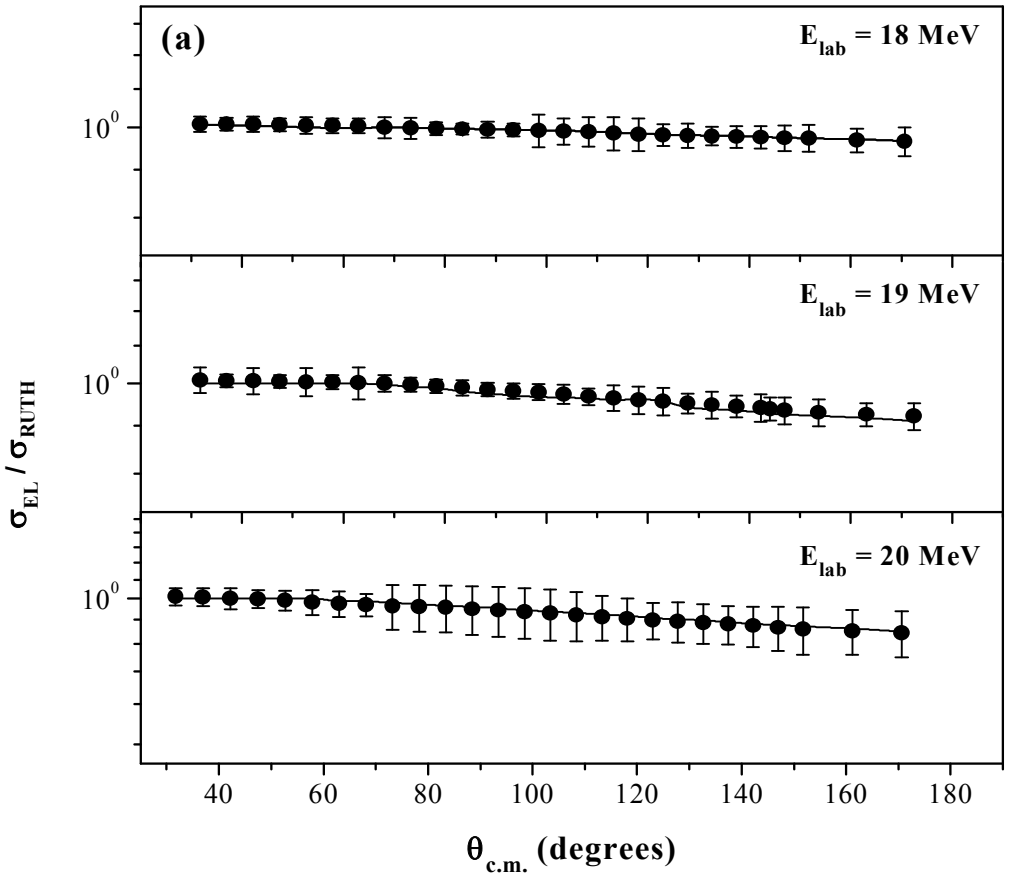

Figure 4.4 (a) Experimental elastic scattering cross sections normalized to the Rutherford cross sections for the ^{7}Li + ^{116}Sn system at energies E_{lab} = 18 – 20 MeV and their best fits from optical model calculations. The curves correspond to best fits were obtained using the Woods – Saxon potential (WSP).

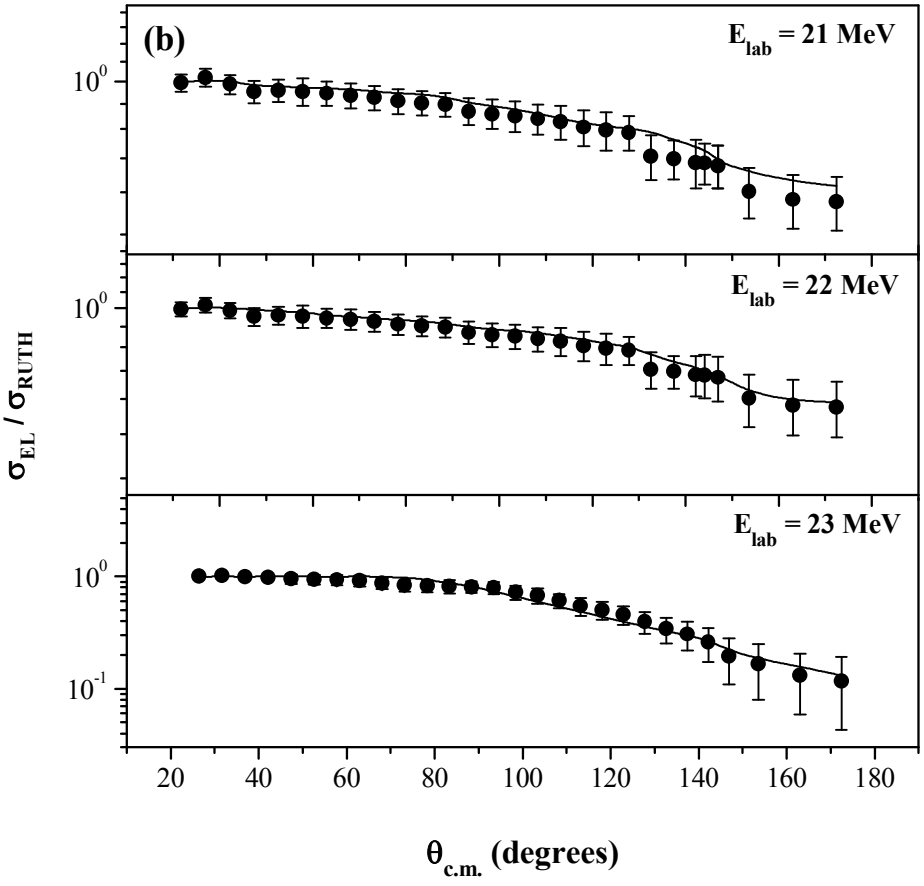

Figure 4.4 (b) Same as Fig. 4.4 (a) but for energies E_{lab} = 21 – 23 MeV.

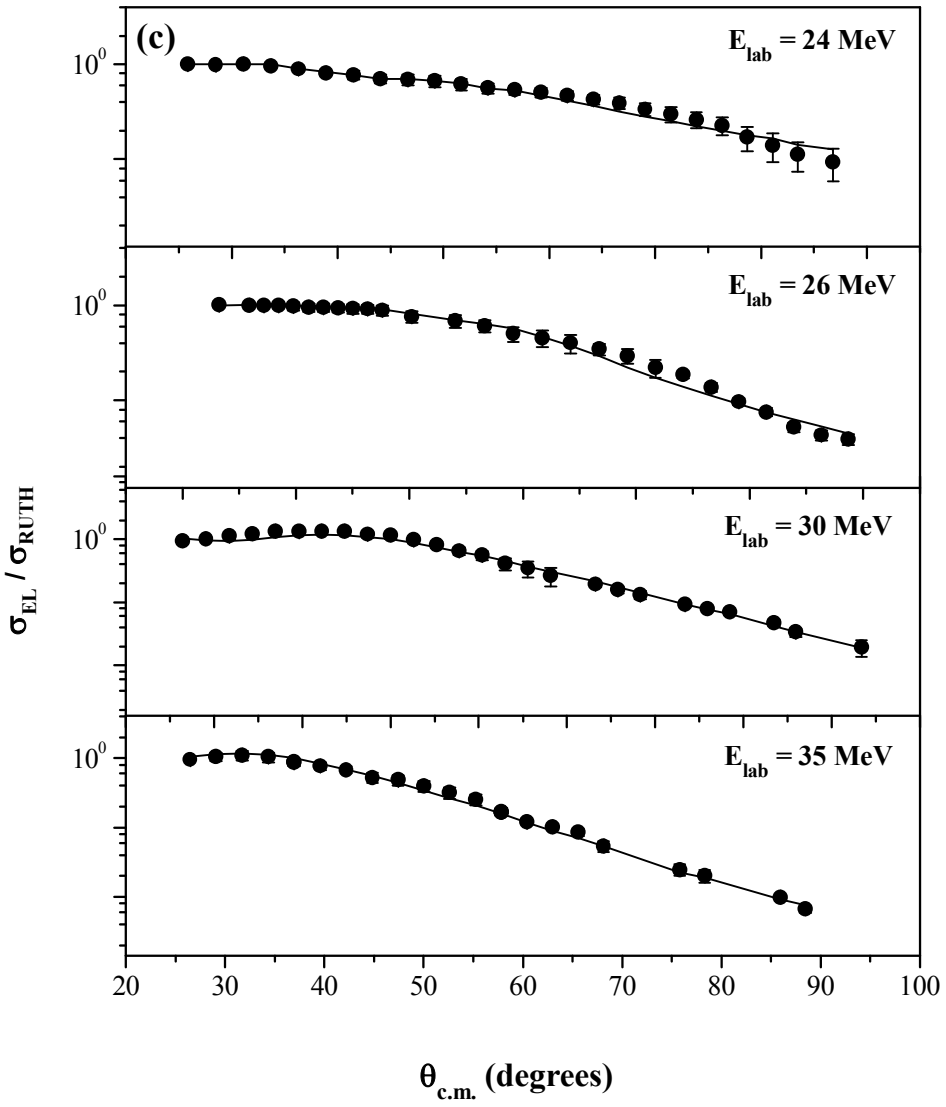

Figure 4.4 (c) Same as Fig. 4.4 (a) but for energies E_{lab} = 24 – 35 MeV.

Table 4.1 Parameters used with Woods – Saxon potential calculations for ^{7}Li + ^{116}Sn System and the derived total reaction cross sections.

E_{lab} (MeV)	V_r (MeV)	V_i (MeV)	R_v & R_i (fm)	a_r & a_i (fm)	χ^2 / n	σ_R (mb)
18	2500	3850	7.20	0.45	0.30	21
19	2550	3450	7.20	0.45	2.32	55
20	2580	3500	7.20	0.45	0.88	128
21	757	901	7.20	0.53	3.10	257
22	550	616	7.20	0. 53	1.33	327
23	349	552	7.20	0. 53	0.67	405
24	855	600	7.20	0. 53	4.00	635
26	498	255	7.20	0. 53	1.71	730
30	565	61	7.20	0. 53	0.81	1059
35	789	31.5	7.20	0. 53	6.83	1444

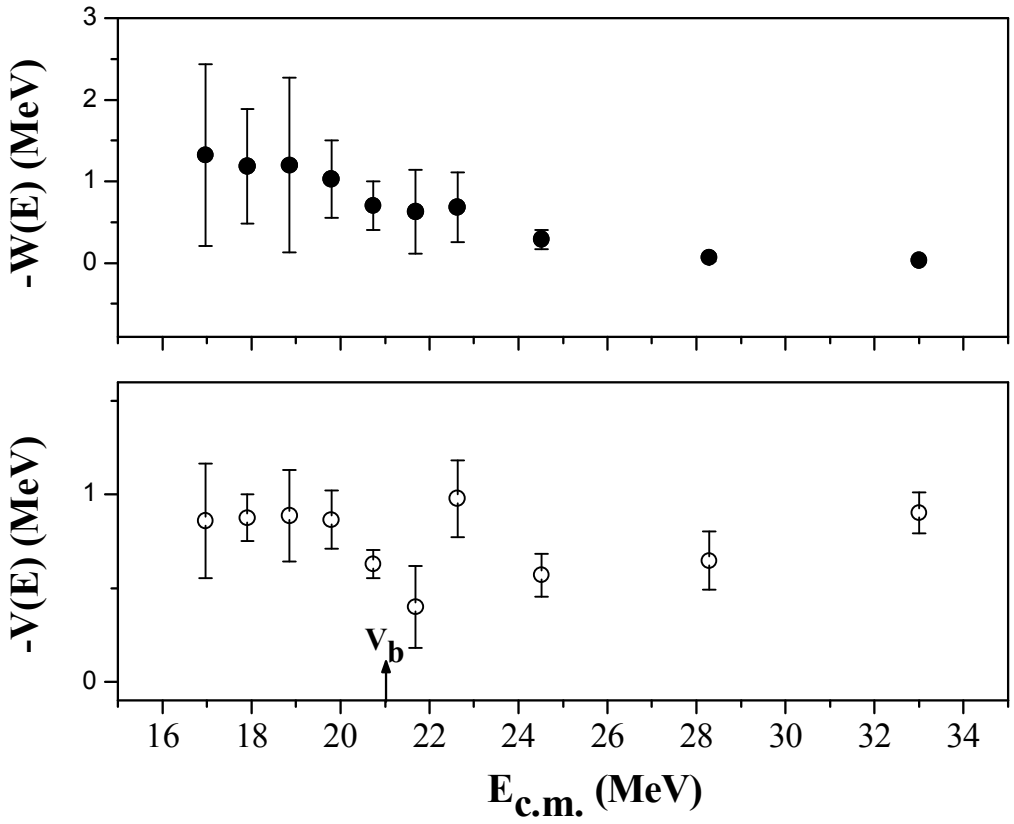

Figure 4.5 Energy dependence of the real and imaginary parts of the optical potential obtained for the ^{7}Li + ^{116}Sn system at an average radius R_s = 9.685 fm. The energy V_b of the Coulomb barrier is shown by the arrow.

From Fig. 4.5 it can be observed that real and imaginary parts of the interacting potentials are quite energy independent at energies higher than the Coulomb energy. However it can be observed that at energies below the Coulomb barrier the imaginary part of the OP does not drop to zero, but rather there is a small increment indicating the absence of the TA. One can also see an almost constant trend of the real potential at lower energies, instead of the characteristic bell shape that corresponds to the TA. This behaviour is very similar to the one observed for the ^{7}Li + ^{144}Sm system [15]. For the much lighter ^{7}Li + ^{27}Al system [21], both the real and imaginary potentials show almost energy independent behaviours. For any of those systems, there is no evidence of the presence of the TA. The BTA behaviour, with a sharp increase of the imaginary potential is also not observed. The explanation for that should be that the attractive polarization potential due to the ^{7}Li bound excited state and transfer channels is of similar strength as the repulsive polarization potential due to the breakup for these systems. Also, very recently it has been shown [30, 31] that an important fraction of the ^{7}Li breakup is not a direct mechanism, but rather a sequential process where the stripping of one neutron and the pickup of one proton take place before the breakup. These first step transfer reactions may decrease the strength of the repulsive breakup polarization potential, as compared with pure direct breakup of ^{7}Li. On the other hand, if one compares the present results with those from our previous measurements of elastic scattering data for the ^{6}Li + ^{116}Sn system [9], one finds that the later has a behaviour more compatible with the BTA, since there is a trend of increasing the imaginary potential at energies below the barrier and some corresponding decrease of the real potential, as the bombarding energy decreases. The reason for these different behaviours between the two Li isotopes should be mainly due to the absence of bound excited state in ^{6}Li and lower threshold energy for breakup than for ^{7}Li. Also, most of the ^{6}Li breakup seems to be direct breakup [30, 32] rather than breakup following transfer.

4.5.2. Analysis Using the Double-Folding Sao Paulo Potential

The São Paulo potential has been employed for fitting of the elastic scattering angular distribution data by using the ECIS code [29]. The Sao Paulo potential [27, 28] is a model for the heavy-ion nuclear interaction. The trivial energy dependence of the bare interaction arises from the use of a local equivalent model based on the nonlocal nature of the interaction. Over a limited

range of energy, as in the present work, it can be considered to be the usual double-folding potential based on an extensive systematization of nuclear densities extracted from elastic scattering data. The imaginary part of the interaction is assumed to have the same shape as the real part, with one single adjustable parameter N_I related to its strength. At near barrier energies, due to the strong energy dependence of the optical potential, the data fit procedure is performed with two free parameters, the normalization factors for the real and imaginary parts, N_R and N_I. Fig. 4.6 shows the experimental elastic scattering angular distributions and the best fit obtained. The results of the energy dependence of the best N_R and N_I values are shown in Fig. 4.7 and can be also found in [33]. It can be observed that the energy dependence (Fig. 4.7) follows the same trend as in the previous analysis. So, our conclusions concerning the behavior of the OP energy dependence do not change when either potential is used. Table 4.2 shows the potential parameters which best fit the data for the ^{7}Li + ^{116}Sn system.

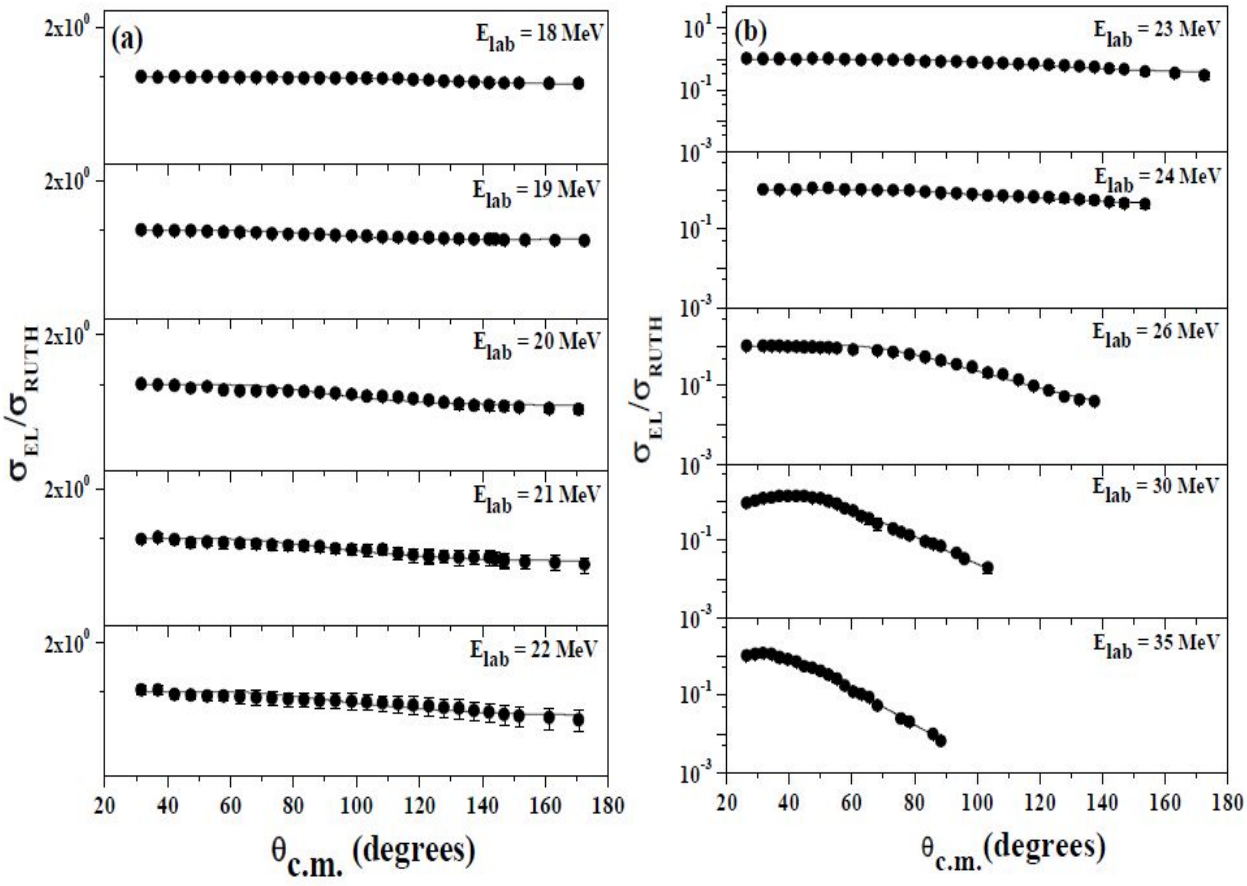

Figure 4.6 Experimental elastic scattering cross sections normalized to Rutherford cross sections for the ^{7}Li + ^{116}Sn system and their best fits from optical model calculations. The curves correspond to best fits were obtained using the Sao Paulo potential (SPP).

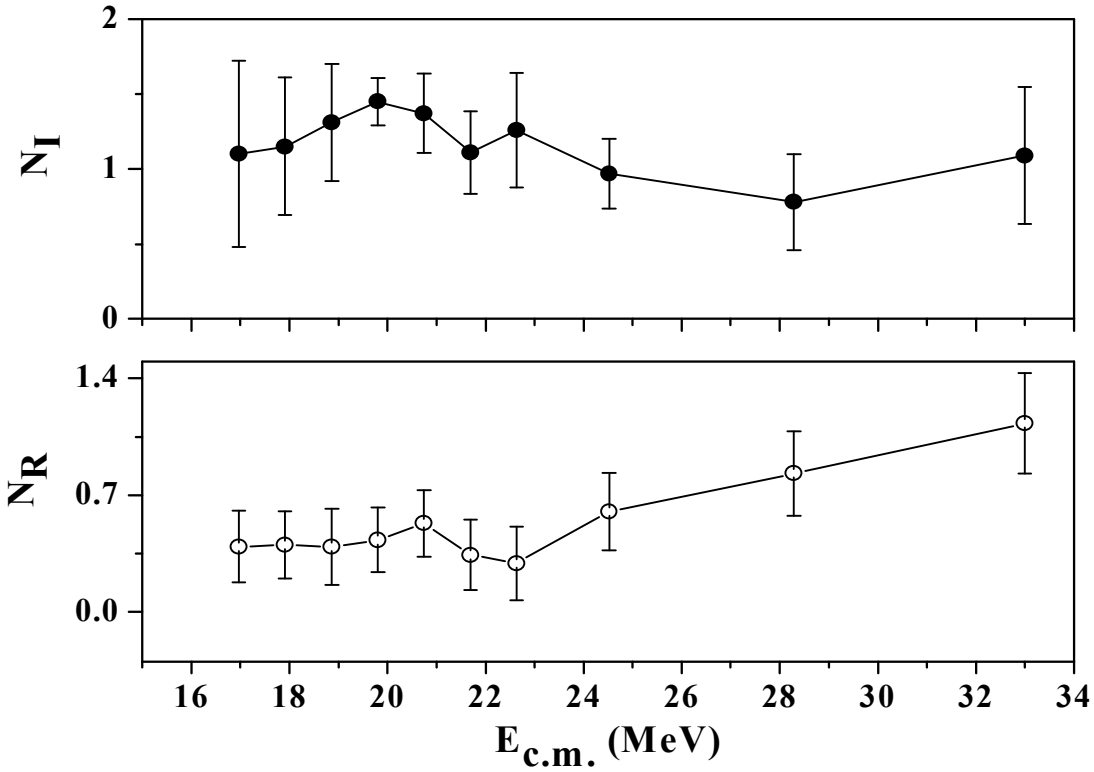

Figure 4.7 Best fits for N_R and N_I as a function of the bombarding energy obtained from fits with the São Paulo potential for the ^{7}Li + ^{116}Sn system. The energy V_b of the Coulomb barrier is around 21.2 MeV in the centre of mass frame calculated using the Bass formula. The solid line is just a trend line to show the dependence of interacting potential on energy.

Table 4.2 Parameters used with the Sao Paulo potential calculations for ^{7}Li + ^{116}Sn System and the derived total reaction cross sections.

E_{Lab} (MeV)	N_R	N_I	χ^2 /n	σ_R (mb)
18	0.39	1.10	0.31	22
19	0.40	1.15	0.35	52
20	0.39	1.31	0.51	131
21	0.43	1.45	0.42	256
22	0.53	1.37	1.20	346
23	0.34	1.11	0.50	412
24	0.29	1.26	0.40	611
26	0.60	0.97	1.22	770
30	0.83	0.78	1.01	1130
35	1.13	1.09	6.18	1556

4.6 Total Reaction Cross Sections

The total reaction cross sections obtained for the ^{7}Li + ^{116}Sn system, which is derived from the optical model fitting of the experimental data is shown in the last column of the table 4.1. In our recent work [9] on the scattering of ^{6}Li on $^{112, 116}$Sn, we have compared the derived total reaction cross sections for those systems with some other weakly and tightly bound systems. In the present paper we compare the total reaction cross sections between the ^{6}Li + ^{116}Sn and ^{7}Li + ^{116}Sn systems. Figs. 4.8 (a) and 4.8 (b) show the comparison by the two reduction methods widely used to compare cross sections of different systems in the same plot. Fig. 4.8 (a) uses the method proposed by Gomes et al. [34] and Fig. 4.8 (b) uses the method proposed by Canto et al. [35,36] for fusion cross sections and later extended by Shorto et al. [37] for total reaction cross sections. A brief description of both methods can be found in ref [9] and in chapter – 3. One can observe that by both methods the total reaction cross section for the ^{6}Li + ^{116}Sn system is larger than for the ^{7}Li + ^{116}Sn system. So, the different behaviour of the energy dependence of the optical potential for these two systems is reflected in the total reaction cross section values. In the ^{6}Li scattering, the breakup plays a more important role than in the ^{7}Li scattering. The breakup cross section for ^{6}Li should be larger than for ^{7}Li, and consequently, the total reaction cross section is larger for reactions induced by ^{6}Li than by ^{7}Li. Further to emphasize the importance of breakup effect on the total reaction cross section, that is, to examine the dependence of the breakup and total reaction cross section in the vicinity of Coulomb barrier, we have also compare [38] our systems using the above two reduction procedures with the available systems (shown in Figs. 4.9 & 4.10) such as ^{6,7}Li + ^{138}Ba [24], ^{6,7}Li + ^{144}Sm [15], ^{9}Be + ^{144}Sm [39], ^{16}0 + ^{144}Sm [40], ^{4,6}He + ^{120}Sn [41], ^{8}Li + ^{120}Sn [42].

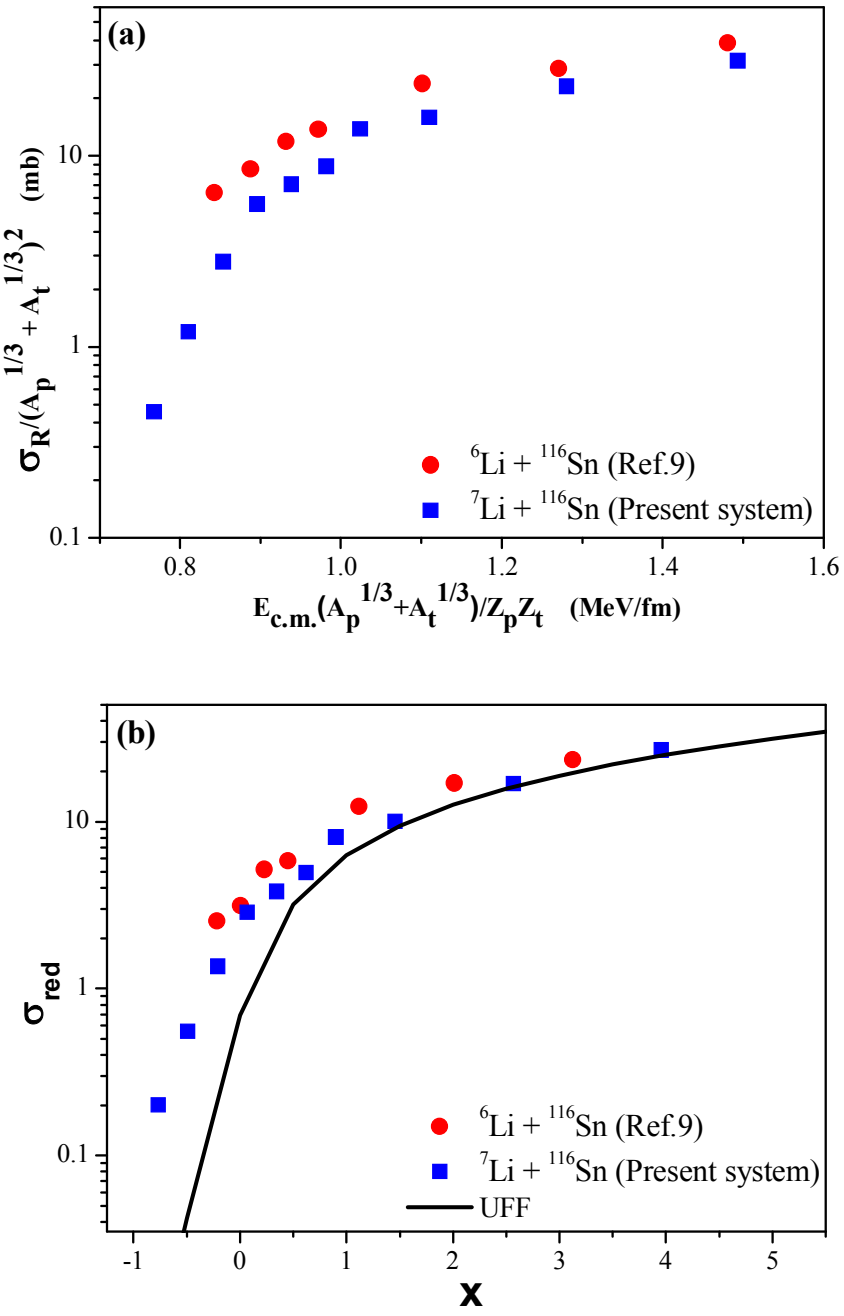

Figure 4.8 Total reaction cross sections for the ^{6,7} Li + ^{116}Sn systems. On the upper panel (a) the reduction method is proposed in Ref. [34] and on the lower panel (b), the reduction method is proposed in ref [35 – 37].

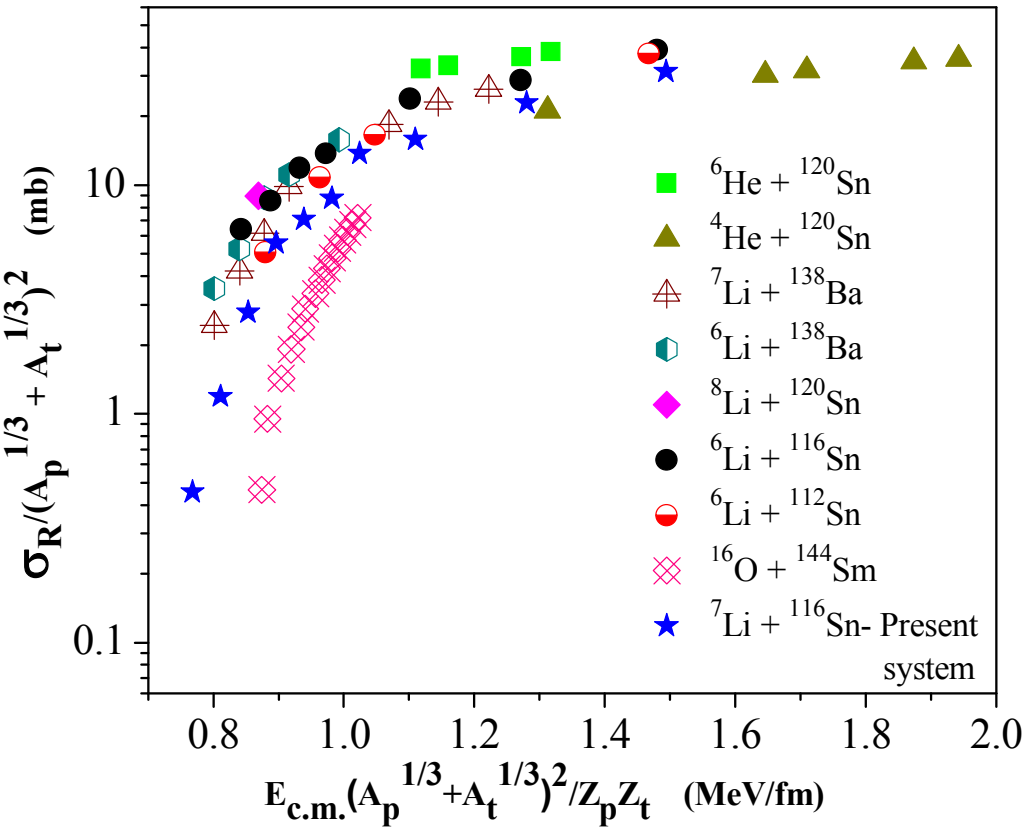

Figure 4.9 Reduced reaction cross section vs reduced projectile energy for the ^{7}Li + ^{116}Sn reaction using the prescription given in Ref. [34]. The reaction cross sections were obtained from optical model fits of the experimental angular distributions.

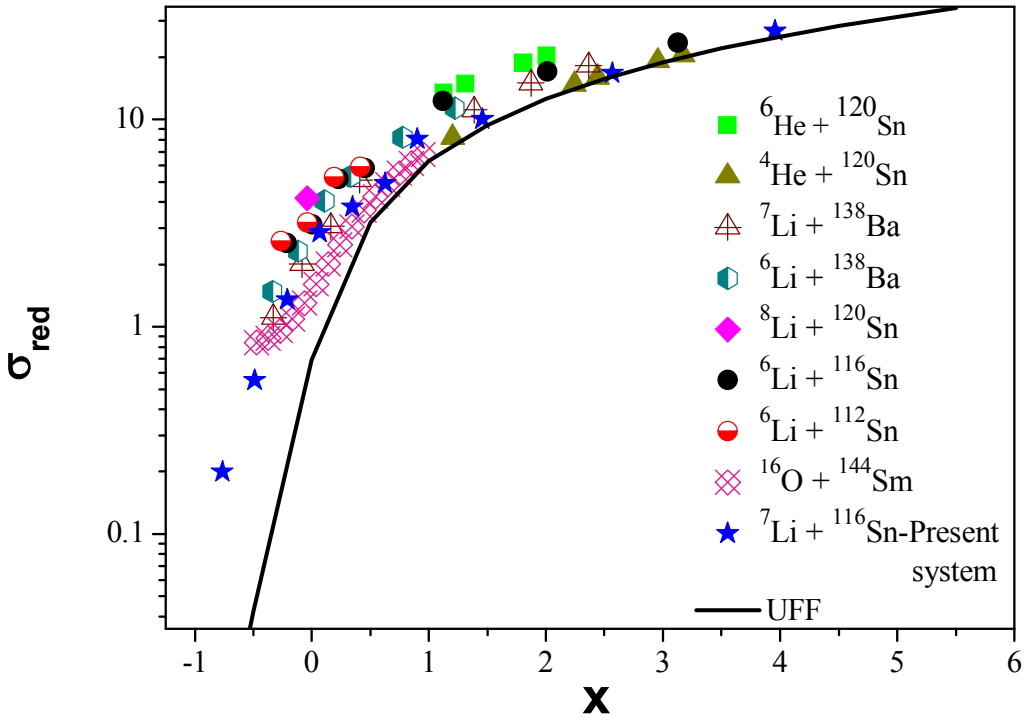

Figure 4.10 Reduced reaction cross section vs reduced projectile energy for the ^{7}Li + ^{116}Sn reaction using the prescription given in Ref. [35 – 37]. The reaction cross sections were obtained from optical model fits of the experimental angular distributions.

4.7 Breakup threshold anomaly in ^{6,7}Li + ^{116}Sn system: A dispersion relation analysis

The energy dependence of the optical potential near the barrier shows consistent behavior in the optical model and double folding framework and it can be tested using dispersion relations [43,44]. The elastic scattering cross section can be reproduced by introducing an effective interaction/optical potential that accounts for all coupling effects and thus the many-body problem can be reduced to a one-body problem with an equivalent potential.

$$U(r,E) = V(r,E) + iW(r,E), \tag{4.3}$$

where V and W are the real and imaginary parts of the potential and are connected through the dispersion relation:

$$\begin{aligned} V(r,E) = {} & V_0(r,E) + \Delta V(r,E), \\ & \Delta V(r,E) = \frac{P}{\pi}\int_0^\infty \frac{W(r,E')}{E'-E}dE', \end{aligned} \tag{4.4}$$

where ΔV is an attractive polarization potential. The imaginary potential W has little effect on ΔV at low energy; therefore V_0 can be normalized at some energy E_s ,

$$\begin{aligned} V(r,E) = {} & V_0(r,E_s) + \frac{P}{\pi}(E-E_s) \\ & \times \int_0^\infty \frac{W(r,E')}{(E'-E_s)(E'-E)}dE'. \end{aligned} \tag{4.5}$$

We have used [45] the linear segment model proposed in Ref. [43] for *W(r,E)* and tried to get the real part. These dispersion relations for phenomenological Woods - Saxon model is given in Figs. 4.11 and 4.12, respectively. The analysis suggests the absence of the threshold anomaly (TA) in ^{6}Li + ^{116}Sn system [9] due to the almost energy independence of the real part of the optical potential. The existence of non – zero imaginary potential even below the Coulomb barrier implies the existence of open reaction channel in this energy region. This result is in agreement with those obtained for the scattering of ^{6}Li by heavier and lighter targets and it show a clear behavior typical of the breakup threshold anomaly (BTA). We explain these behaviors by the fact that the scattering of weakly bound nuclei are affected by the repulsive polarization

potential produced by the breakup process, important even at energies below the Coulomb barrier. However, for ^{7}Li + ^{116}Sn [25] scattering the energy dependence behavior of the imaginary potential seems to differ from those in the literature for several other systems involving ^{7}Li as a projectile. In this case there is a strong competition between this repulsive polarization potential and the attractive polarization potential produced by the bound ^{7}Li excited state and transfer reactions. These two components of the real polarization potential may have similar strengths and the net result could give rise to an almost energy independent real part. And the non – zero imaginary part at the sub – barrier energies might have resulted due to the dominant breakup channel similar to ^{6}Li.

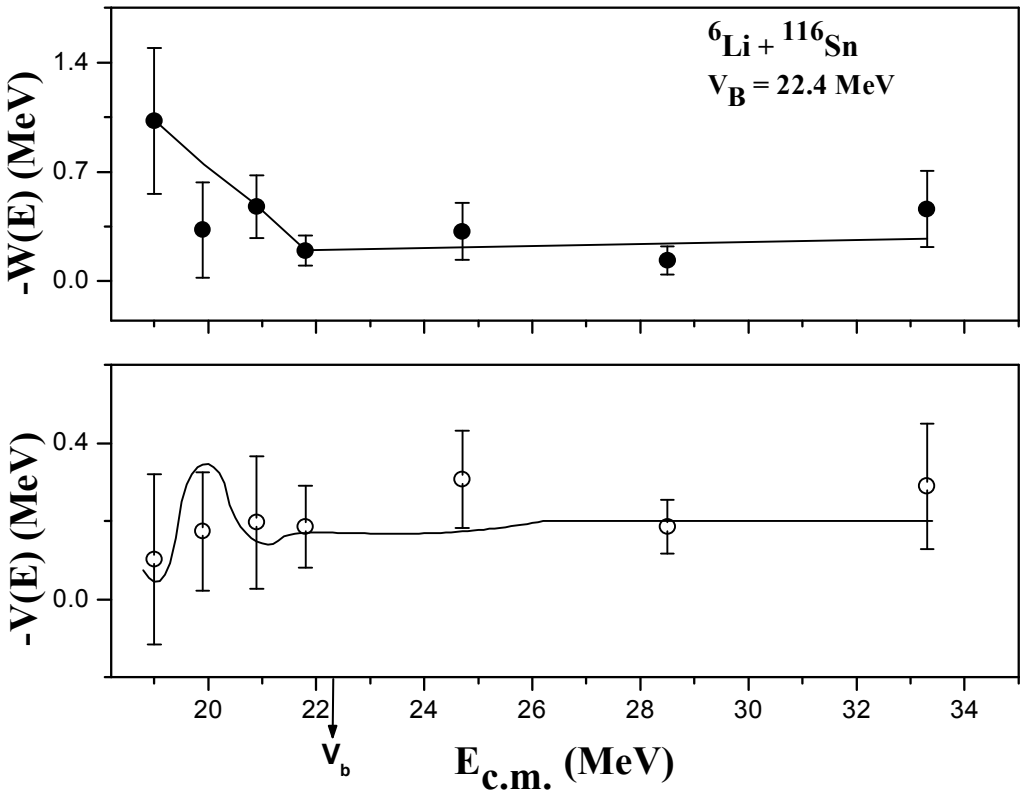

Figure 4.11 Values of the imaginary and real parts of the optical potential at the average sensitive radius, equal to 9.40 fm, for the system ^{6}Li + ^{116}Sn. The solid line corresponds to the dispersion relation calculations.

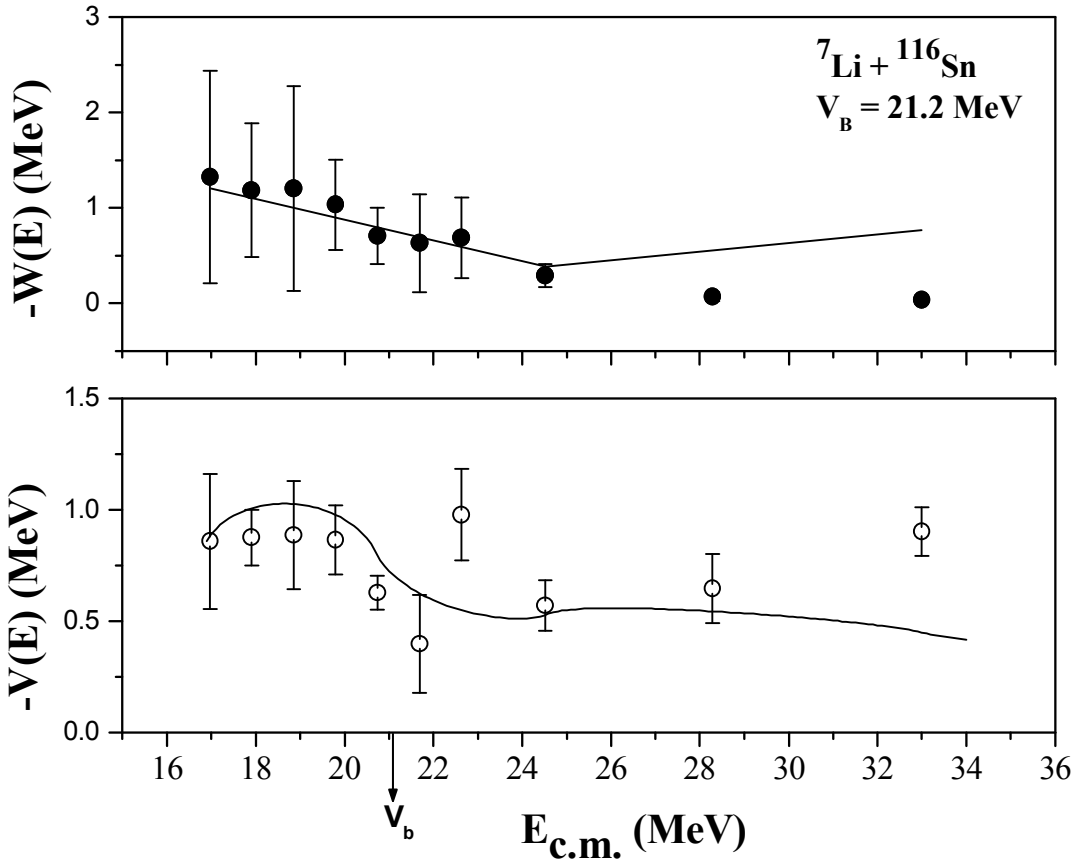

Figure 4.12 Values of the imaginary and real parts of the optical potential at the average sensitive radius, equal to 9.685 fm, for the system ^{7}Li + ^{116}Sn. The solid line corresponds to the dispersion relation calculations.

4.8 Conclusions

In order to contribute to the investigation of the presence of the threshold anomaly or breakup threshold anomaly in the optical potential of the scattering of weakly bound systems, elastic scattering angular distributions have been measured for the ^{7}Li + ^{116}Sn system at energies around and below the Coulomb barrier. The present analysis suggests the absence of the threshold anomaly (TA) due to the almost energy independence of the real and imaginary parts of the optical potential. This result is in agreement with those obtained for the scattering of ^{7}Li by heavier and lighter targets. On the other hand, several systems with ^{6}Li as projectile show a clear behaviour typical of the threshold breakup anomaly (BTA), including the one with the same ^{116}Sn target. We explain these behaviours by the fact that the scattering of weakly bound nuclei are affected by the repulsive polarization potential produced by the breakup process, important even at energies below the Coulomb barrier, but for the specific case of ^{7}Li there is a strong competition between this repulsive polarization potential and the attractive polarization potential produced by the bound ^{7}Li excited state and transfer reactions. For ^{7}Li, these two components of the polarization potential have similar strengths and the net result is an almost energy independent optical potential. This result cannot be extrapolated for every target, because the relative importance of the polarization potential produced by the different reaction mechanisms may vary with the target structure. The total reaction cross section for the ^{6}Li + ^{116}Sn system is larger than for ^{7}Li + ^{116}Sn system, corresponding to larger breakup cross section for the former than for the later. This work also reports the comparison of our system with the several other systems using the two reduction methods. The total reaction cross-sections for all systems, and by the two reducing methods used, were found to be similar, irrespective of the projectile being tightly or weakly bound, stable or radioactive, except when halo nuclei were present. In this situation, the total reaction sections were larger than for the others. Dispersion relation analysis for the two systems, that is, ^{6}Li + ^{116}Sn and ^{7}Li + ^{116}Sn, has been also done to check the energy dependence of the optical potential near the barrier. From this analysis too, the clear – cut presence of BTA could be observed for both the systems.

References

[1] M.A. Nagarajan, C.C. Mahaux, G.R. Satchler, Phys. Rev. Lett. **54**, 1136 (1985).

[2] G.R. Satchler, Phys. Rep. **199**, 147 (1991).

[3] M.E. Brandan, G.R. Satchler, Phys. Rep. **285**, 143 (1997).

[4] P.R.S. Gomes *et al*., J. Phys. G **31**, S1669 (2005).

[5] M.S. Hussein *et al*., Phys. Rev. C **73**, 044610 (2006).

[6] M.S. Hussein, P.R.S. Gomes, J. Lubian, L.C.Chamon, private communication.

[7] K. Zerva *et al*., Phys. Rev. C **80**, 017601 (2009).

[8] K. Zerva *et al*., Phys. Rev. C **82**, 044607 (2010).

[9] N. N. Deshmukh *et al.,* Phys. Rev. C **83**, 024607 (2011).

[10] J.M. Figueira *et al*., Phys. Rev. C **75**, 017602 (2007).

[11] A. Gomez Camacho *et al*., Nucl. Phys. A **833**, 156 (2010)

[12] M. Biswas *et al*., Nucl. Phys. A **802**, 67 (2008).

[13] M. Zadro *et al*., Phys. Rev. C **80**, 064610 (2009).

[14] H. Kumawat *et al.,* Phys. Rec. C **78**, 044617 (2008).

[15] J.M. Figueira *et al*., Phys. Rev. C **81**, 024613 (2010).

[16] N. Keeley *et al*., Nucl. Phys. A **571**, 326 (1994).

[17] S. Santra *et al*., Phys. Rev. C **83**, 034616 (2011).

[18] J. Lubian *et al.,* Nucl. Phys. A **791,** 24 (2007).

[19] A. Pakou *et al*., Phys. Lett. B **556**, 21 (2003).

[20] A. Pakou *et al*., Phys. Rev. C **69**, 054602 (2004);

[21] J.M. Figueira *et al*., Phys. Rev. C **73**, 054603 (2006).

[22] F. A. Souza *et al*., Phys. Rev. C **75**, 044601 (2007).

[23] J. Lubian *et al*., Phys. Rev. C **64**, 027601 (2001).

[24] A.M.M. Maciel *et al*., Phys. Rev. C **59**, 2103 (1999).

[25] N.N. Deshmukh *et al*., Eur. Phys. J A **47**, 118 (2011).

[26] J. Ziegler, www.srim.org

[27] L.C. Chamon *et al*., Phys. Rev. Lett. **79**, 5218(1997).

[28] L.C. Chamon *et al*., Phys. Rev. C **66**, 014610 (2002).

[29] J. Raynal, Phys. Rev. C **23**, 2571 (1981).

[30] D. H. Luang *et al*., Phys. Lett. B **695**, 105 (2011).

[31] D. Martinez Heimann *et al*., Nucl. Instr. Meth. In Phys. Res. A **622**, 642 (2010).

[32] O.A. Capurro *et al*., Nucl. Phys. A **849**, 1 (2011).

[33] N.N. Deshmukh *et al*., AIP Conference Proceedings, **1423**, 122 – 125 (2012) (IX – Latin America Symposium on Nuclear Physics and Applications, 2011).

[34] P.R.S. Gomes *et al*., Phys. Rev. C **71**, 017601 (2005).

[35] L.F. Canto *et al*., J. Phys. G 36, 015109 (2009)

[36] L.F. Canto *et al*., Nucl. Phys. A **821**, 51 (2009)

[37] J.M. B. Shorto *et al*., Phys. Lett. B **678**, 77 (2009).

[38] N.N. Deshmukh *et al*., Proceedings of National Conference on Emerging Interfaces of Physics and Technology – 2011 (EIPT – 2011), Excel India Publishers (ISBN: 978-93-81361-31-3), Page 108 – 111.

[39] P.R.S. Gomes *et al*., Nucl. Phys. A **828**, 233 (2009)

[40] J. R. Leigh *et al.*, Phys. Rev. C **52**, 3151 (1995).

[41] P.N. de Faria *et al*., Phys. Rev. C **81**, 044605 (2010).

[42] P.N. de Faria, Ph.D. thesis, IFUSP, 2009.

[43] C. Mahaux, H. Ngô, and G. R. Satchler, Nucl. Phys. A **449**, 354 (1986).

[44] G. R. Satchler, Nucl. Phys. A **472**, 591 (1987).

[45] N.N. Deshmukh *et al*., Proceedings of the DAE Symposium on Nuclear Physics, Vol. **56**, Page 478 – 479 (2011).